Comparison of Nanocomposites Prepared from Sodium, Zinc, and Lithium Ionomers of Ethylene/Methacrylic Acid Copolymers

Rhutesh K. Shah and D. R. Paul*

Department of Chemical Engineering and Texas Materials Institute, The University of Texas at Austin, Austin, Texas 78712

Received January 2, 2006; Revised Manuscript Received March 3, 2006

ABSTRACT: Morphology and mechanical properties of nanocomposites prepared by melt mixing a montmorillonite-based organoclay with lithium, sodium, and zinc ionomers of poly(ethylene-*co*-methacrylic acid) are presented here. The effect of the type of neutralizing cation on the melt rheology and organoclay exfoliation efficiency of the ionomers was examined using transmission electron microscopy, wide-angle X-ray scattering, DSM axial-force rheometry, and stress−strain analysis. Nanocomposites prepared from the sodium and the zinc ionomers displayed much better exfoliation of the organoclay and superior levels of reinforcement compared to equivalent nanocomposites prepared from the lithium ionomer. On the basis of the detailed experimental analysis, the lower levels of organoclay exfoliation observed in the nanocomposites prepared from the lithium ionomer are suggested to be a result of irreversible exchange of quaternary ammonium ions (of the organoclay) for the very small lithium ions (of the polymer) that can enter the montmorillonite lattice structure.

Introduction

A commercially important class of ionomers consists of random copolymers of ethylene and methacrylic acid where some of the acid groups are neutralized to form metal salts.[1] Typically, the methacrylic acid content of these polymers is low (<15 mol %), and the degree of neutralization ranges from 20 to 80%. The resulting polymer structure has three regions: amorphous and crystalline phases plus ionic clusters.[2] The incorporation of the ionic groups improves the toughness, melt viscosity, clarity, and adhesion properties of the copolymer.[3] As a result, these ionomers are extensively used in a variety of applications ranging from orthotics and prosthetics to packaging and sealants and from glass coatings to outer coverings for golf balls and bowling pins.[4]

Recently, nanocomposites prepared by melt mixing such ionomers with organically modified montmorillonite clays (organoclays) have attracted a great deal of technological and scientific interest because of their potential for significant improvements in physical and barrier properties at low filler levels.[5−7] The key to achieving these benefits is exfoliating the organoclay into the polymer matrix to generate high aspect ratio particles. In this regard, ethylene/methacrylic acid ionomers have a distinct advantage over the base polyolefin, low-density polyethylene (LDPE). The presence of the pendant ionic groups and the polar methacrylic acid groups in these ionomers potentially creates favorable interactions between the polymer and the aluminosilicate clays, resulting in a much more exfoliated morphology compared to nanocomposites prepared from LDPE.[7] Nanocomposites prepared from ionomers of polypropylene,[8] poly(ethylene terephthalate),[9,10] poly(butylene terephthalate),[10,11] and a variety of other nonpolar thermoplastics polymers[12−14] also reveal good levels of organoclay exfoliation.

In this study, we examine the effect of the type of neutralizing cation on the exfoliation efficiency of the ion-containing polymer and on the morphology and mechanical properties of the nanocomposites formed. Sodium, zinc, and lithium ionomers of poly(ethylene-*co*-methacrylic) acid were carefully chosen such that all other specifications, viz., melt index, acid content, and degree of neutralization, are comparable. Nanocomposites were prepared by melt mixing these ionomers with an appropriate organoclay in a twin-screw extruder. Stress−strain analysis, X-ray scattering (WAXS), and transmission electron microscopy (TEM) coupled with particle analysis were used to evaluate the level of organoclay exfoliation, and appropriate mechanisms have been suggested to explain the differences in the rheology, morphology, and properties of these nanocomposites.

Experimental Section

Materials. Three commercial grades of Surlyn ionomer resins, Surlyn 7940, 8945, and 9945, were purchased from du Pont. These are lithium, sodium, and zinc salts, respectively, of poly(ethylene-*co*-methacrylic acid). As shown in Table 1, all three polymers have similar melt indices, acid contents, and degrees of neutralization.

The organically modified clay, designated here as $M_2(HT)_2$, was generously donated by Southern Clay Products and was used as received. It was prepared by a cation exchange reaction between sodium montmorillonite (Na-MMT) and a two-tailed quaternary ammonium surfactant, dimethyl bis(hydrogenated-tallow) ammonium choloride (Arquad 2HT-75). Selected properties of this organoclay are also included in Table 1. The choice of the organoclay was based on a recent study exploring the effect of surfactant structure on organoclay exfoliation in sodium ionomers of poly(ethylene-*co*-methacrylic acid).[15] The study revealed that higher levels of organoclay exfoliation could be achieved using surfactants with multiple alkyl tails on the ammonium ion rather than one tail. This is believed to be the result of the better affinity these ionomers have for the largely aliphatic organic modifier than for the pristine surface of the clay. In addition, the larger the number of alkyl tails, the more the silicate surface is shielded from the matrix; this combination of factors leads to better exfoliation of an organoclay having multiple alkyl tails.

Melt Processing. Melt compounded composites were prepared using a Haake, corotating, intermeshing twin-screw extruder (diameter = 30 mm, $L/D = 10$) using a barrel temperature of 190 °C and a screw speed of 280 rpm. The polymers and the organoclays were premixed and fed to the extruder using a single hopper. As in the past,[15] the feed rate was initially set at 1200 g/h. However, the high melt viscosities generated in the case of a few nanocom-

* Corresponding author: Tel 512-471-5392; Fax 512-471-0542; e-mail drp@che.utexas.edu.

10.1021/ma0600052 CCC: $33.50
Published on Web 03/31/2006

Table 1. Materials Used in This Study

material	commercial designation	specifications	supplier
zinc ionomer of poly(ethylene-*co*-methacrylic acid)	Surlyn 9945	MI = 4.1 g/10 min specific gravity = 0.97 methacrylic acid content = 15.0 wt % zinc oxide content = 3.70 wt % neutralization = ~40%	E.I. du Pont de Nemours and Company
sodium ionomer of poly(ethylene-*co*-methacrylic acid)	Surlyn 8945	MI = 4.5 g/10 min specific gravity = 0.96 methacrylic acid content = 15.2 sodium content = 1.99 wt % neutralization = ~40%	E.I. du Pont de Nemours and Company
lithium ionomer of poly(ethylene-*co*-methacrylic acid)	Surlyn 7940	MI = 2.66 g/10 min specific gravity = 0.94 methacrylic acid content = 14.7 wt % lithium content = 0.52 wt % neutralization = ~40%	E.I. du Pont de Nemours and Company
organoclay:[a] dimethyl bis(hydrogenated-tallow) ammonium montmorillonite	Cloisite 20A	organic loading = 95 mequiv/100 g clay organic content = 39.6 wt % d_{001} spacing[b] = 25.5 Å	Southern Clay Products

[a] The selected organoclay is designated as $M_2(HT)_2$ in this study, where M = methyl and HT = hydrogenated tallow. Tallow is a natural product composed predominantly (63%) of saturated and unsaturated C_{18} chains. HT is the saturated form yet still contains a small fraction of double bonds. [b] The basal spacing corresponds to the characteristic Bragg reflection peak d_{001} obtained from a powder WAXS scan of the organoclay.

posites based on the zinc ionomer (containing more than 5 wt % MMT) resulted in high values of extruder torque that exceeded the permissible limits of the equipment. Hence, all nanocomposites evaluated in this study were prepared using a lower feed rate of 800 g/h. Surlyn materials were dried in a vacuum oven at 65 °C for a minimum of 48 h prior to compounding while the organoclays were used as received. In prior studies from this laboratory,[16,17] the amount of montmorillonite in the nanocomposite was determined by placing predried nanocomposite pellets in a furnace at 900 °C for 45 min and weighing the remaining MMT ash. It was not possible to employ this technique with these ionomers since the polymer itself resulted in a hard, yellowish-green coating on the inside of the crucible reflecting some complex residue of the inorganic component of the ionomer. The amount of the residue varied from batch to batch, rendering this method useless for quantitative analysis. Hence, to ensure that a predetermined polymer/MMT ratio was maintained in all cases, the desired amounts of clay and polymer were premixed before feeding to the extruder, and precautions were taken to minimize any losses of organoclay during the extrusion process.

Tensile specimens (ASTM D638) were prepared by injection molding using an Arburg Allrounder 305-210-700 injection molding machine using a barrel temperature of 220 °C, mold temperature of 45 °C, injection pressure of 70 bar, and a holding pressure of 40 bar. After molding, the samples were immediately sealed in a polyethylene bag and placed in a vacuum desiccator for a minimum of 24 h prior to testing. The samples made from the three unfilled ionomers were colorless and clear. On the other hand, the injection-molded nanocomposite samples had a yellowish tint, the intensity of which increased with the clay content. There were visible differences between the clarity of the nanocomposites prepared from the three ionomers. Nanocomposite samples prepared from the sodium and the zinc ionomers maintained the clarity of the unfilled polymer samples. In contrast, the clarity of the samples prepared from the lithium ionomer decreased as the clay content increased; this reflects the poorer exfoliation of organoclay in this matrix.

Testing and Characterization. Tensile tests were conducted at room temperature according to ASTM D696 using an Instron model 1137 machine equipped with digital data acquisition capabilities. Modulus was measured using an extensiometer at a crosshead speed of 0.51 cm/min. Elongation at break and tensile strength at break were measured at a crosshead speed of 5.1 cm/min. Typically, data from six specimens were averaged to determine the tensile properties with standard deviations of the order of 2−7% for modulus, 1−10% for tensile strength at break and, 2−21% for elongation at break. Yield stress data are not reported because the stress−strain behavior of some of the nanocomposites do not show a distinct yield point.

Relative melt viscosities of the polymers and their nanocomposites were determined using a DSM microcompounder (chamber volume = 5 cm^3) operated under "recycle" mode. Prior to testing, the polymers and their nanocomposites were dried in a vacuum oven at 65 °C for ~48 h. A charge of 2.5 g of polymer/nanocomposite pellets was mixed separately in the microcompounder using a constant screw speed of 100 rpm at 190 °C. The axial force, which is a function of the melt viscosity, was recorded at regular intervals over a 10 min period.

WAXD was conducted using a Sintag XDS 2000 diffractometer in the reflection mode with an incident X-ray wavelength of 1.542 Å at a scan rate of 1.0°/min. X-ray analysis was performed at room temperature on injection-molded Izod bars. The specimens were oriented such that the incident beam reflected off the major face.

Samples for TEM analysis were taken from the core portion of an Izod bar parallel to the flow direction but perpendicular to the major face. Ultrathin sections ~50 nm in thickness were cut with a diamond knife at a temperature of −65 °C using a Reichert-Jung Ultracut E microtome. Sections were collected on 300 mesh grids and subsequently dried with filter paper. These were then examined using a JEOL 2010F TEM equipped with a field emission gun at an accelerating voltage of 120 kV at a magnification of 25K. The negative films containing the electron micrographs were electronically scanned and converted into gray scale tagged-image file format (TIFF) files, and the images were subsequently printed on a 20.3 × 25.4 cm^2 photographic paper. To conduct quantitative analysis on these images, the lengths, thicknesses, and aspect ratios of the particles were determined. The lengths of the particles were traced manually on a transparency film using a felt tip pen, and the resultant tracings were scanned and converted into TIFF files. The thickness of the dispersed platelets and agglomerates were traced digitally on an overlapped blank layer in Adobe Photoshop under high magnification. Thus, two separate tracings were done for each TEM picture: one contained the lengths of the particles, and the other one contained their thicknesses. The resulting black and white layer files were then imported into an image analysis software, Scion Image, which analyzed the traced particles, assigned a numerical label to each of them, and exported their characteristic dimensions to a different file. Since two different tracings were used for measuring the lengths and thicknesses of the particles, each particle got assigned two different numerical labels. This made it extremely difficult to match the length of a given particle with its thickness

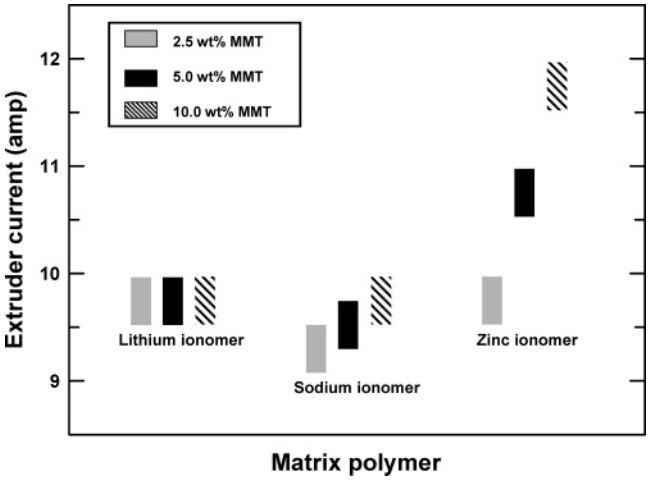

Figure 1. Electrical current drawn by the extruder motor during extrusion of the various nanocomposites based on ionomers of ethylene/methacrylic acid copolymers. The feed (polymer + organoclay) rate in all cases is 800 g/h.

and, thus, calculate the aspect ratio of a particular particle. Hence, in this study, the particle aspect ratio for any given nanocomposite was determined by dividing the average particle length by the average particle thickness.[18−20]

Observations and Results

Processability and Rheology. Figure 1 shows the electrical current drawn by the extruder motor while processing the various nanocomposites based on lithium, sodium, and zinc ionomers of poly(ethylene-*co*-methacrylic acid) at a feed rate of 800 g/h. At a fixed screw speed, the current drawn is a function of the torque, which in turn is dependent upon the melt viscosity of the nanocomposite being processed. For nanocomposites prepared from the lithium ionomer, the current does not change much with clay concentration. For the nanocomposites based on the sodium ionomer, there is a small increase in the current when the clay content is gradually increased from 2.5 wt % MMT to 10.0 wt % MMT. The slightly lower current observed for the nanocomposites made from the sodium ionomer, compared to those formed from the lithium ionomer at low filler concentrations, could be a result of the small difference in the melt indices of the two matrices (4.5 g/10 min vs 2.6 g/10 min). In contrast, the current for the nanocomposites based on the zinc ionomer increases steadily, but significantly, when the montmorillonite content is increased from 2.5 to 10 wt %, which is indicative of a large increase in melt viscosity as the clay content is increased.

To get a rough idea of the comparative melt viscosities, we decided to measure the relative viscosities of the unfilled polymers and their nanocomposites using a DSM microcompounder, as described in the Experimental Section. Figure 2a compares the axial force generated by the polymer melts when sheared at 190 °C using a screw speed of 100 rpm in a DSM microcompounder. Initially (t < 90 s), the forces decrease with time for all three ionomers. The differences between the forces generated by the three polymer melts in this region could be attributed to the small differences in their melt indices. Between t = 90 s and t = 600 s, there is little change in the axial force generated by the lithium and sodium ionomer melts; however, the force exerted by the zinc ionomer melt increases steadily to a value which is ∼25% higher than the minimum observed at t < 90 s. Although we are not completely sure what causes this increase in the melt viscosity of the zinc ionomers, we believe it is a result of possible formation of anhydrides in the polymer

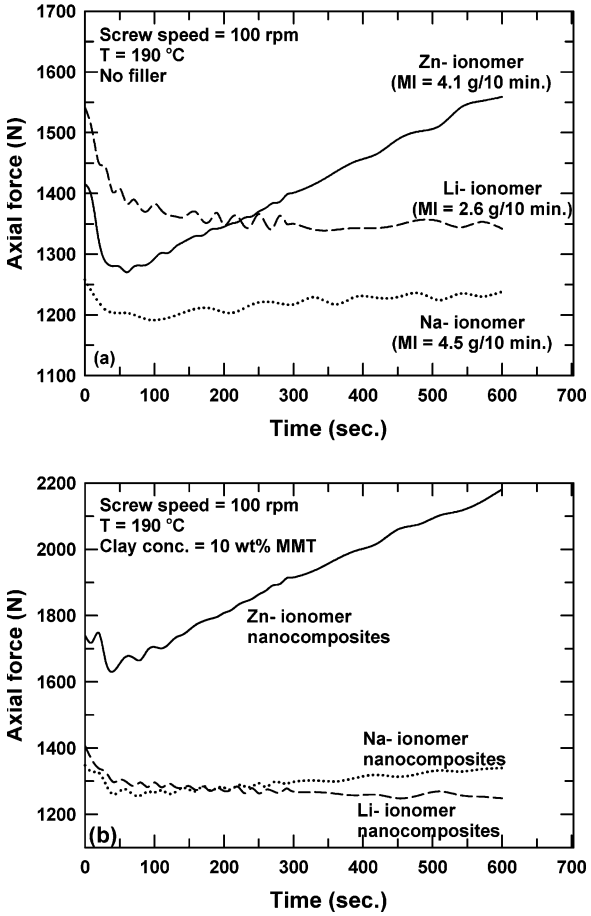

Figure 2. Axial forces generated by (a) the ionomers and (b) nanocomposites containing 10 wt % MMT prepared from these ionomers, when sheared at 190 °C using a screw speed of 100 rpm in a DSM microcompounder.

melt. As mentioned in Table 1, the degree of neutralization of the ionomers used in this study is about 40%. The remaining unneutralized acid groups are capable of forming anhydrides (with the expulsion of water); these anhydrides could act as branch (and eventually cross-link) points, which could lead to an increase in the melt viscosity of the polymer. Transition metal salts (such as zinc acetate) are well-known to catalyze anhydride formation, just as they act as esterification catalysts. So, it could be that this process is more rapid for Zn ionomers than Li and Na ionomers.[21,22] Small amounts of water in the polymer could affect the anhydride formation reaction. In this study, the pellets were dried in a vacuum oven prior to testing, as described in the Experimental Section; however, no additional precautions were taken to prevent the absorption of moisture during the weighing and charging of polymers to the microcompounder. Also, no special steps were taken to prevent or facilitate the removal of water vapor from the partially filled chamber during the melt mixing process.

The nanocomposites prepared from these ionomers exhibited similar trends as shown in Figure 2b. Careful comparison of parts a and b of Figure 2 suggests that, while the axial forces generated by the nanocomposites prepared from sodium and zinc ionomers are higher than those of the corresponding unfilled polymers, the nanocomposite based on the lithium ionomer produces a smaller viscous force than the lithium ionomer itself. The higher melt viscosities of the sodium and zinc ionomer nanocomposites could be an artifact of organoclay exfoliation in these polymers, while the lower melt viscosity of the Li ionomer nanocomposites could be a consequence of composi-

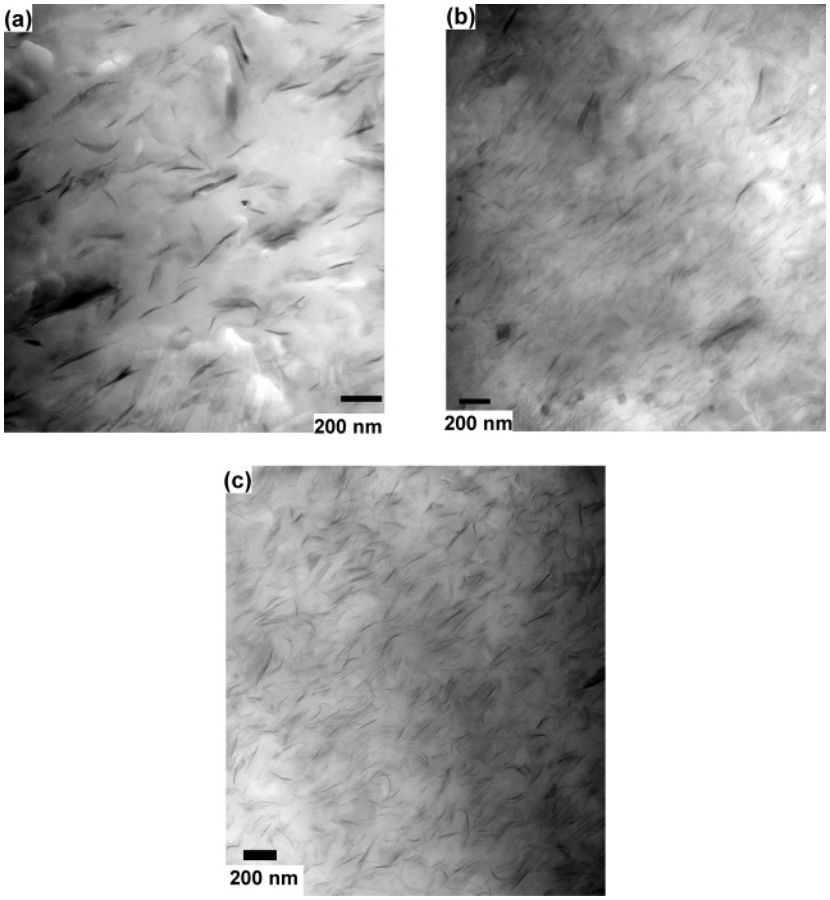

Figure 3. TEM micrographs of nanocomposites prepared from $M_2(HT)_2$ organoclay and (a) lithium, (b) sodium, and (c) zinc ionomers of poly(ethylene-*co*-methacrylic acid). The concentration of MMT in all three cases is ~5 wt %. Sections were microtomed from the core portion of an Izod bar in a plane parallel to the flow direction but perpendicular to the major face.

tional changes of the organoclay that are unique to mixing with the lithium ionomer as described later.

The results of this limited rheological evaluation of the polymers and their nanocomposites suggest a more comprehensive rheological study; however, this is beyond the scope of this paper.

TEM and Particle Analysis. Figure 3 shows TEM micrographs comparing the morphology of nanocomposites formed from $M_2(HT)_2$ organoclay and lithium, sodium, and zinc ionomers of poly(ethylene-*co*-methacrylic acid). The concentration of montmorillonite in all three samples is 5 wt %. Nanocomposites prepared from the sodium ionomer (Figure 3b) and the zinc ionomer (Figure 3c) exhibit better clay exfoliation or dispersion of the organoclay than the one prepared from the lithium ionomer (Figure 3a). The micrographs of nanocomposites prepared from the former two reveal a pattern of uniformly dispersed single platelets along with a few thin stacks comprised of 2−4 platelets. On the other hand, the morphology of the lithium ionomer based nanocomposites revealed a significant number of thicker stacks of platelets.

To provide a quantitative comparison of the level of organoclay exfoliation in the three matrices, particle analysis was conducted on TEM micrographs of nanocomposites using image analysis techniques as described in the Experimental Section and in previous studies.[18−20,23] Figure 4 shows a series of histograms of MMT particle lengths and pertinent statistical data obtained on nanocomposites containing ~5 wt % MMT prepared from $M_2(HT)_2$ organoclay and the three ionomers. The sections were taken parallel to the flow direction but perpendicular to the major face. Similar measurements were conducted for the thickness of clay particles, and the results are plotted in Figure 5. The filler particles in the nanocomposites prepared from the sodium and the zinc ionomer were shorter and thinner than the ones in the nanocomposites based on the lithium ionomer. The average particle length of ~92 nm calculated in the case of the former two nanocomposites agrees well with the average particle length in well-exfoliated nylon-6 nanocomposites determined using a similar technique.[18] It is interesting to note the greater average particle length in the nanocomposite prepared from the lithium ionomer (163 nm) compared to similar nanocomposites prepared from the sodium and zinc ionomers (92 nm). This could be a result of a partial breakdown of the clay agglomerates comprised of randomly overlaid platelets and the "skewing" of thicker clay bundles as described by Chavarria et al.[19] The thickness distribution profiles of particles in the nanocomposites prepared from the sodium ionomer and the zinc ionomer appear to be fairly similar, with ~75% of the particles having a thickness of 4 nm or less. Their average particle thickness (~3.5 nm) was noticeably lower than that calculated for the nanocomposites based on the lithium ionomer (11.9 nm). The aspect ratio of the particles in each nanocomposite was determined by dividing the average particle length by the average particle thickness of the nanocomposite (see Table 2). The average particle aspect ratio in the nanocomposites based on the sodium ionomer and the zinc ionomer was calculated to be ~27, while that in the nanocomposites based on the lithium ionomer was determined to be ~14. On the basis of the TEM evaluation and particle analysis, it can be concluded that (i) the sodium and the zinc ionomers are much more efficient at exfoliating the $M_2(HT)_2$ organoclay than the lithium ionomer

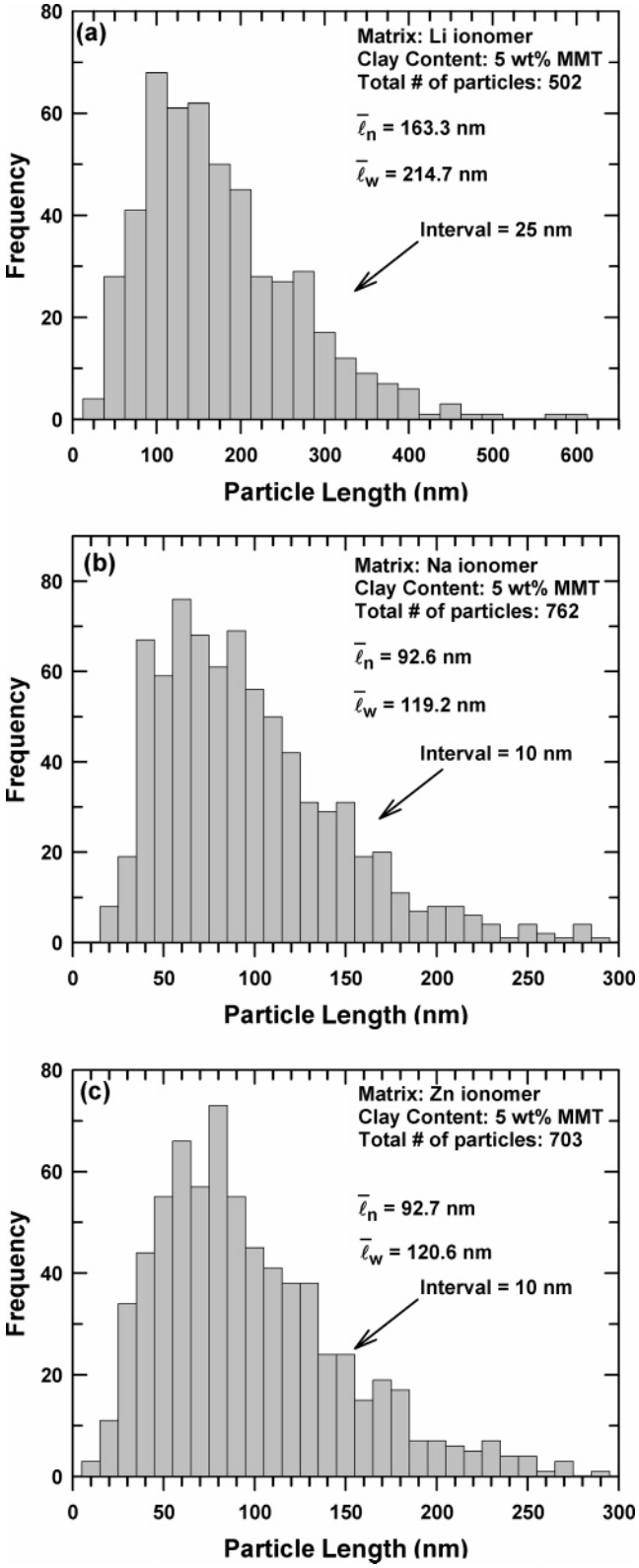

Figure 4. Histograms of MMT particle length obtained by analyzing TEM micrographs of nanocomposites containing ~5 wt % MMT prepared from (a) lithium, (b) sodium, and (c) zinc ionomers of poly(ethylene-*co*-methacrylic acid).

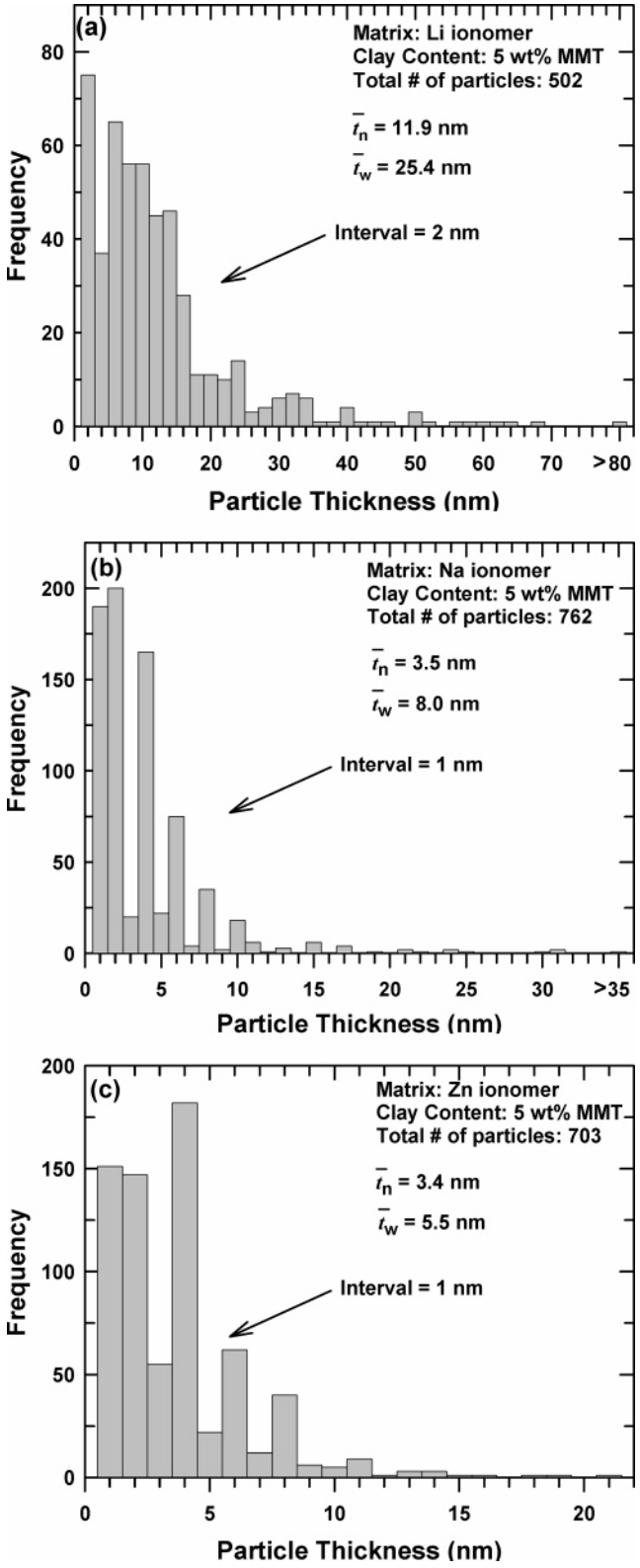

Figure 5. Histograms of MMT particle thickness obtained by analyzing TEM micrographs of nanocomposites containing ~5 wt % MMT prepared from (a) lithium, (b) sodium, and (c) zinc ionomers of poly(ethylene-*co*-methacrylic acid).

and (ii) there is not much difference in the morphology of the nanocomposites (containing 5 wt % MMT) prepared from the sodium and the zinc ionomer.

Mechanical Properties. Selected mechanical properties of the nanocomposites prepared are listed in Table 3. However, before we discuss these properties in detail, it is important to highlight the similarities and subtle differences in the stress−strain behavior of these composites. Figure 6 displays typical stress−strain diagrams for nanocomposites prepared from $M_2(HT)_2$ organoclay and lithium, sodium, and zinc ionomers. The stress−strain curves of the unfilled lithium and sodium ionomers reveal a distinct stress maximum followed by a slight drop in

Table 2. Particle Analysis Results

organoclay nanocomposites	total no. of particles	number-average particle length (nm)	weight-average particle length (nm)	number-average particle thickness (nm)	weight-average particle thickness (nm)	aspect ratio[a]	aspect ratio[b]
lithium ionomer (Surlyn 7940) + 5 wt % MMT	502	163.3	214.7	11.9	25.4	13.7	8.4
sodium ionomer (Surlyn 8945) + 5 wt % MMT	762	92.6	119.2	3.5	8.0	26.5	14.9
zinc ionomer (Surlyn 9945) + 5 wt % MMT	703	92.7	120.6	3.4	5.5	27.3	21.9

[a] These values of the aspect ratio were computed from the number-average platelet lengths and thicknesses. [b] These values of the aspect ratio were computed from the weight-average platelet lengths and thicknesses.

Table 3. Selected Mechanical Properties of Nanocomposites Prepared by Melt Mixing $M_2(HT)_2$ Organoclay and Ionomers of Poly(ethylene-*co*-methacrylic acid)

polymer	montmorillonite content (wt %)	tensile modulus, E (GPa)	relative modulus, E/E_m	elongation at break (5.1 cm/min) (%)	tensile strength at break (5.1 cm/min) (MPa)
zinc ionomer	0.0	0.176	1.00	172	19.3
zinc ionomer	2.5	0.314	1.78	116	22.2
zinc ionomer	5.0	0.447	2.50	85.9	24.2
zinc ionomer	10.0	0.795	4.51	58.9	29.2
sodium ionomer	0.0	0.260	1.00	194	21.0
sodium ionomer	2.5	0.412	1.58	130	22.6
sodium ionomer	5.0	0.568	2.18	119	25.9
sodium ionomer	10.0	0.908	3.49	65.6	28.8
lithium ionomer	0.0	0.292	1.00	136	21.0
lithium ionomer	2.5	0.407	1.38	116	24.2
lithium ionomer	5.0	0.491	1.68	104	24.8
lithium ionomer	10.0	0.676	2.32	98.4	27.2

the tensile stress after this yield point, corresponding to the onset of necking. This stress drop gradually diminishes as the clay content increases. In contrast, the stress−strain curves of the zinc ionomer and nanocomposites prepared from it do not show a maximum stress or a yield point. The stress−strain curves of almost all polymers/nanocomposites suggest the occurrence of strain hardening. The slope of the plastic region, indicative of the level of strain hardening, decreases as the clay content increases.

Figure 7a compares the tensile moduli of the different nanocomposites as a function of their montmorillonite content. As expected, the stiffness of all ionomers improves substantially with addition of $M_2(HT)_2$ organoclay. To get a comparative idea of the improvements in the level of reinforcement achieved, the relative moduli of the nanocomposites are plotted against the montmorillonite content in Figure 7b. It is clear that the increase in modulus observed in nanocomposites prepared from the sodium and zinc ionomers is much greater than that observed in nanocomposites prepared from the lithium ionomer. However, the level of reinforcement observed in nanocomposites formed from the zinc ionomer seems to be somewhat greater than that seen for those formed from the sodium ionomer. These differences are more pronounced at higher MMT content. Thus, it appears that the moduli data are not in complete agreement with the results of the particle analysis, which revealed similar aspect ratios for the zinc ionomer and sodium ionomer-based nanocomposites containing 5 wt % MMT. We are not completely sure about the cause of this disagreement between the results of the two analytical methods. In principle, some part of this discrepancy could stem from differences between the moduli of the two ionomers (0.176 GPa vs 0.260 GPa). Composite theory predicts that for a given filler aspect ratio low-modulus matrices offer greater potential for reinforcement per unit mass of filler than high-modulus matrices due to the larger ratio of filler modulus to the matrix modulus.[24,25] However, simple calculations using the Halpin−Tsai theory reveal that the discrepancy noted above cannot be fully rationalized in this way.[26,27] But then again, these calculations are based upon numerous simplifications and assumptions of ideal conditions.[26]

Another explanation may stem from some departure from one of the basic premises of composite theory; i.e., the matrix modulus is not altered by the presence of the nanoscale clay particles.[24,25] It was suggested above that anhydride formation occurs in nanocomposite based on the zinc ionomer but not those containing sodium or lithium. This chemistry might possibly alter the material properties as clay is added. There seems to be no simple or straightforward way to test such a hypothesis. Finally, a certain degree of caution should be exercised when attempting to correlate mechanical properties with morphology determined by TEM since each micrograph provides a snapshot of only a small microscopic area. An extensive particle analysis is needed to fully describe the morphology of the macroscopic sample which is reflected in property measurements like modulus.

The comparatively smaller improvements in the modulus of the lithium ionomer by addition of the organoclay is a result of the relatively lower levels of organoclay exfoliation in these systems compared to nanocomposites prepared from the zinc and lithium ionomers (as revealed by TEM micrographs). The slightly higher modulus of the unfilled lithium ionomer compared to the other two polymers contributes to some degree to this observation; we propose an additional explanation below.

The relationship between the MMT content of the nanocomposites and their elongation at break is shown in Figure 8. The more exfoliated and stiffer nanocomposites prepared from the zinc and sodium ionomers are less ductile than the relatively less exfoliated nanocomposites prepared from the lithium ionomer; generally, ductility decreases when stiffness is increased by reinforcement.[7,15,28] Also, as mentioned in the Introduction, the presence of the ionic clusters in these ionomers improves their toughness compared to corresponding ethylene/methacrylic acid copolymers. It is unclear whether the ductility of the ionomers is lowered due to possible disruption of the ionic aggregates by the exfoliated/partially exfoliated clay particles.

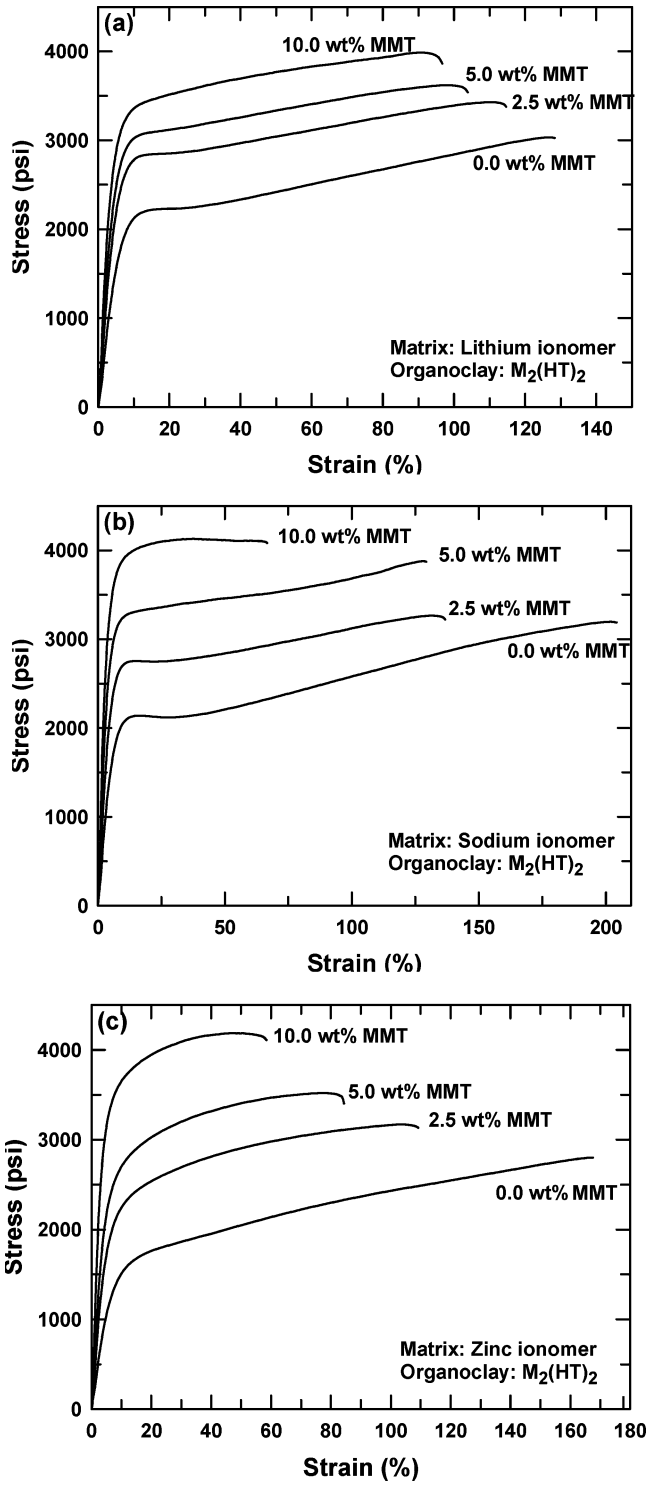

Figure 6. Representative stress−strain diagrams of nanocomposites prepared from $M_2(HT)_2$ organoclay and (a) lithium, (b) sodium, and (c) zinc ionomers of poly(ethylene-*co*-methacrylic acid).

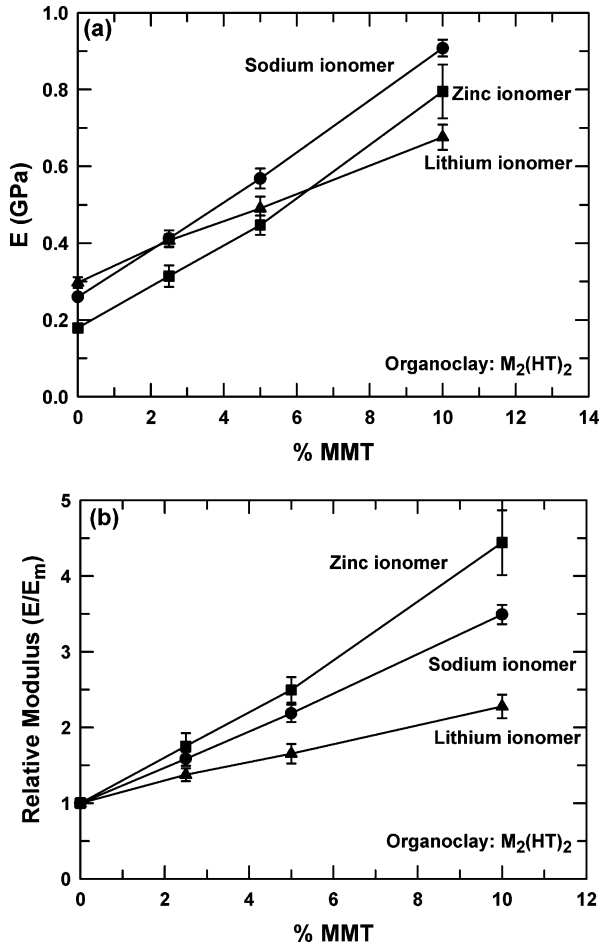

Figure 7. (a) Tensile modulus and (b) relative modulus of nanocomposites prepared from lithium, sodium, and zinc ionomers of poly(ethylene-*co*-methacrylic acid).

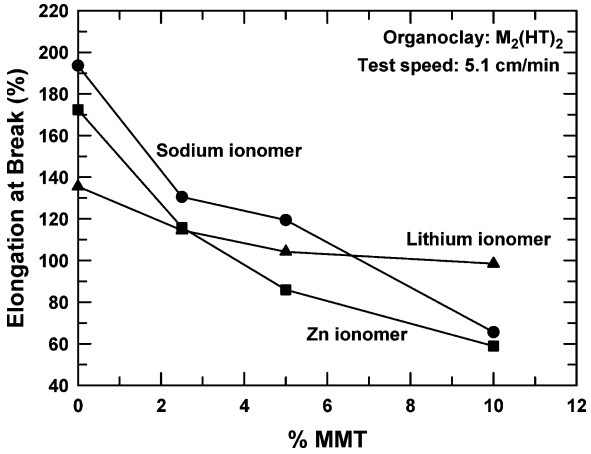

Figure 8. Elongation at break measured at a crosshead speed of 5.1 cm/min for nanocomposites prepared from lithium, sodium, and zinc ionomers of poly(ethylene-*co*-methacrylic acid).

WAXS Analysis. Figure 9 compares the WAXS scans of the $M_2(HT)_2$ organoclay and its nanocomposites prepared by melt mixing with the three ionomer matrices. The organoclay pattern reveals an intense peak at around $2\theta = 3.46°$, corresponding to a basal spacing of 25.5 Å. WAXS patterns of all nanocomposites show a distinct peak indicative of the presence of unexfoliated clay tactoids. However, the positions of the peaks for the nanocomposites shift in different directions relative to the peak of the organoclay. The peaks for composites formed from the zinc and sodium ionomers are shifted to higher *d* spacings than the organoclay, which according to prevalent understanding suggests the intercalation of mass, e.g., polymer, within the clay galleries. On the other hand, the peak for the nanocomposite prepared from the lithium ionomer is shifted to the right (lower *d* spacings), suggesting loss of mass from the galleries, e.g., loss of surfactant mass by degradation or some other mechanism.[29] A detailed description and a proposed mechanism for this phenomenon resulting from the interactions between the lithium ionomer and the filler are described below.

The position of the peak did not change with organoclay content of the nanocomposites; however, the height of the peak

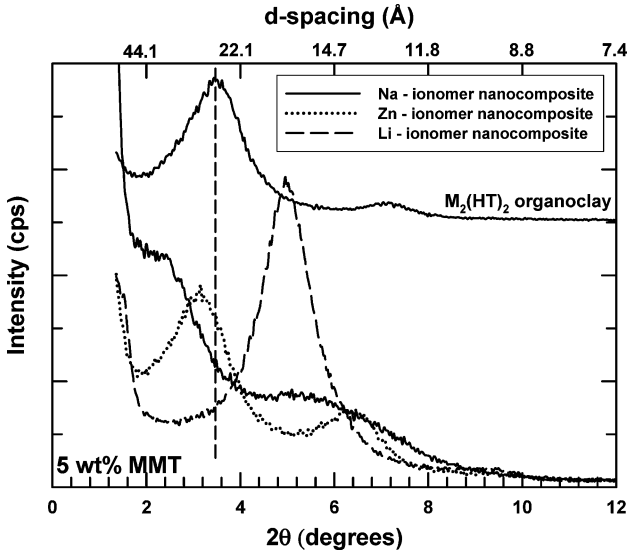

Figure 9. WAXS patterns of nanocomposites prepared from $M_2(HT)_2$ organoclay and the three ionomers. The concentration of MMT in all cases is ~5 wt %. X-ray pattern of the $M_2(HT)_2$ organoclay is plotted for comparison and is shifted vertically for clarity. The dotted vertical line shows the position of the d_{001} peak of the organoclay.

increases as the clay concentration increases, as shown in Figure 10. WAXS results for nanocomposites prepared from unmodified polyethylene exhibit similar trends.[23]

Discussion

As described above, a series of polymer−silicate nanocomposites were prepared by melt mixing $M_2(HT)_2$ organoclay with lithium, sodium, and zinc ionomers of poly(ethylene-*co*-methacrylic acid). Three observations merit special consideration: (i) Unlike the nanocomposites prepared from the sodium and the zinc ionomers, the melt viscosity of the nanocomposite prepared from the lithium ionomer was lower than that of the matrix polymer. (ii) Nanocomposites prepared from the zinc and the sodium ionomers exhibited a higher level of organoclay exfoliation compared to equivalent nanocomposites prepared from the lithium ionomer. (iii) WAXS peaks of the nanocomposites prepared from the sodium and the zinc ionomers shifted to the left (higher *d* spacing), whereas those based on the lithium ionomer shifted to the right (lower *d* spacing).

The right shift of the WAXS peak of a nanocomposite is indicative of a decrease in the interplatelet spacing of the organoclay and is generally attributed to the loss of mass from the organoclay galleries, e.g., by thermal degradation of the surfactant.[29,30] The quaternary ammonium surfactants used for preparing the organoclays are known to degrade at the high temperatures required to melt process the nanocomposites. The initial thermal degradation, which is believed to follow a Hoffman elimination mechanism,[31−33] begins at temperatures as low as 155−165 °C. WAXS patterns of similar nanocomposites prepared from polyethylene,[29] polypropylene,[29] polystyrene,[30] and nylon-66[19] have also revealed such shifts to the right. For LDPE/ $M_2(HT)_2$ nanocomposites, the X-ray peak shifts to 23.2 Å when melt processed at 200 °C.[29] Increasing the processing temperature to 240 °C results in a further decrease in the organoclay *d* spacing (22 Å). For the nanocomposites prepared from the lithium ionomer at 190 °C, the organoclay *d* spacing is reduced much more significantly (from 25.5 to 17.4 Å) compared to that reported for nanocomposites prepared from other polymers using a similar organoclay.[29] It is important to note that WAXS patterns of nanocomposites prepared from the

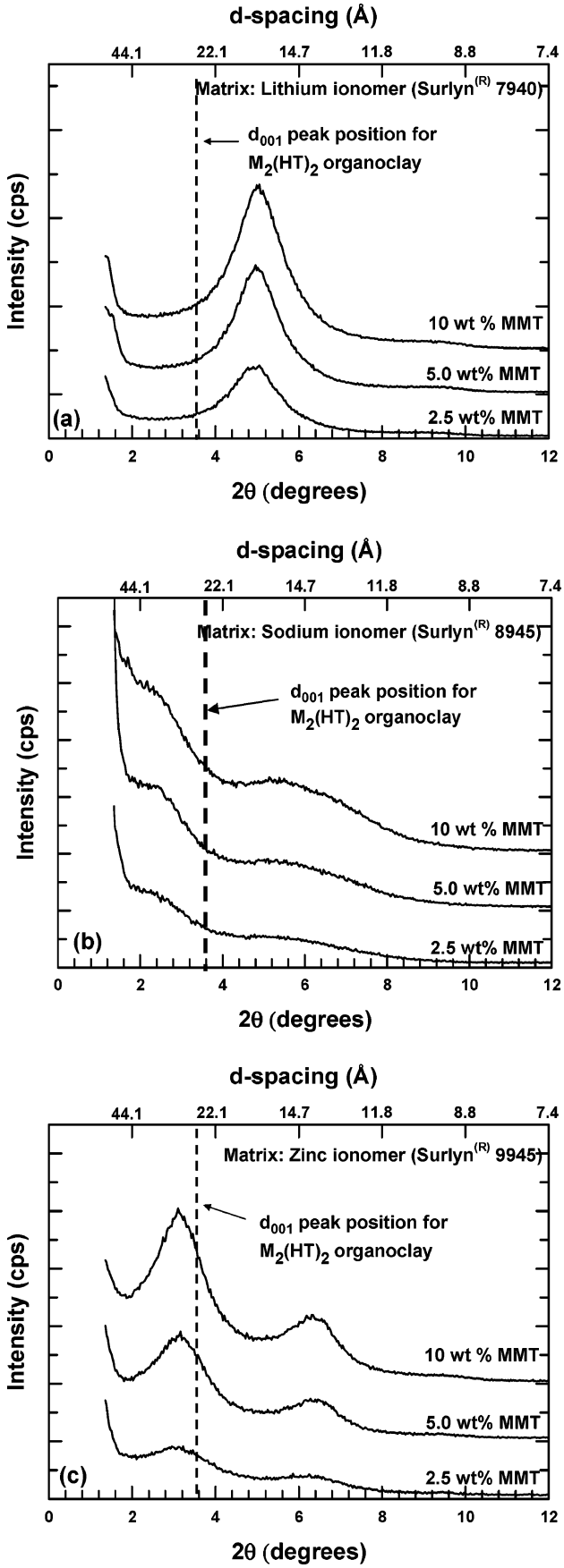

Figure 10. WAXS patterns of nanocomposites prepared from $M_2(HT)_2$ organoclay and (a) lithium, (b) sodium, and (c) zinc ionomers of poly(ethylene-*co*-methacrylic acid). The dotted vertical line showing the position of the d_{001} peak of the $M_2(HT)_2$ organoclay is included for comparison. The curves are shifted vertically for clarity.

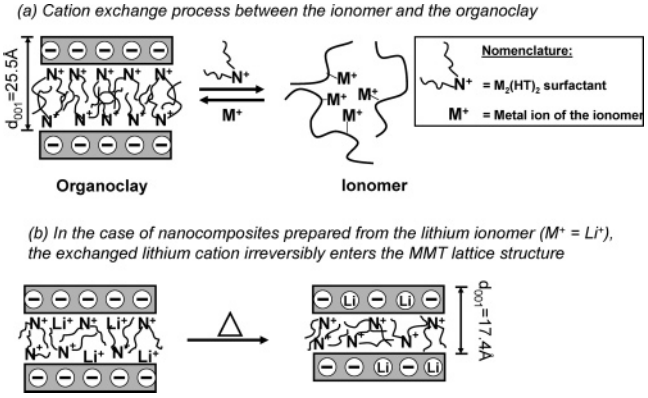

Figure 11. Schematic of the proposed ion-exchange process between the ionomer and the organoclay which subsequently leads to a reduction in the *d* spacing of the nanocomposites prepared from the lithium ionomer.

zinc and the sodium ionomers do not reveal such peak shifts. As far as we know, there are no reports of the catalytic effects of the Li^+ ion on the Hoffman elimination reaction. Thus, it appears that for the nanocomposites based on the lithium ionomer there may be another mechanism than thermal degradation of the surfactant by the Hoffman elimination reaction involved in the shift of WAXS peak to higher *d* spacings.

A possible explanation may involve an ion exchange process between the organoclay and these ionomers, wherein a few of the bulky quaternary ammonium ions of the organoclay are replaced by the smaller metal cations of the ionomers, thus reducing the *d* spacing of the organoclay as shown in Figure 11. The obvious question is, why is such behavior only exhibited by the nanocomposites prepared from the lithium ionomer and not by the nanocomposites prepared from the sodium and the zinc ionomers? The answer possibly lies in the smaller size and the higher reactivity of the lithium cation. The Li^+ ion has a radius of 0.68 Å compared to 0.74 Å for the Zn^{2+} ion and 0.98 Å for the Na^+ ion. The Li^+ ion is capable of entering the montmorillonite lattice structure, resulting in an irreversible exchange of quaternary ammonium ions.[34−41] Hofmann and Klemen[34] showed that heating Li^+-saturated bentonite caused fixation of previously exchangeable Li^+ ions and a reduction of the cation exchange capacity (CEC) and expandability of the main clay mineral present in bentonite (Hofmann−Klemen effect). The irreversible exchange of the Li^+ ions could serve as a driving force for the cation exchange process between the organoclay and the ionomer. On the other hand, Zn^{2+} and Na^+ ions are not as capable of entering the montmorillonite lattice structure as the Li^+ ions. Emmerich et al.,[42,43] while investigating homoionic forms of montmorillonite heated at 220 °C for 20 h, found that the CEC of the Li^+ forms of montmorillonite dropped to 28% of the value observed in an unheated sample. In comparison, the CEC of Zn^{2+} form dropped marginally to 91%, and there was no change in the CEC of the Na^+ form. Thus, in the case of nanocomposites prepared from the sodium and the zinc ionomers, there is no driving force to promote the cation exchange reaction between the polymer and the organoclay.

The cation exchange process and the relatively lower levels of organoclay exfoliation could also explain why nanocomposites prepared from the lithium ionomer do not show similar improvements in melt viscosity over that of the unfilled ionomer as those revealed by nanocomposites prepared from the sodium and the zinc ionomers. Replacement of the smaller Li^+ cations by bulkier quaternary ammonium cations in the polymer phase should affect the melt rheology of the nanocomposite.

Conclusion

Structure−property relationships for nanocomposites prepared from ionomers of poly(ethylene-*co*-methacrylic acid) and $M_2(HT)_2$ organoclay have been presented here. The effect of the neutralizing cation on the exfoliation efficiency of the polymer was evaluated by comparing the morphology and properties of nanocomposites prepared from sodium, zinc, and lithium ionomers of poly(ethylene-*co*-methacrylic acid). On the basis of transmission electron microscopy and particle analysis of the images, nanocomposites prepared from the zinc and the sodium ionomers show much better exfoliation of the organoclay compared to equivalent nanocomposites prepared from the lithium ionomer. The mechanical properties of the nanocomposites paralleled the TEM observations in this regard. WAXS peaks of the sodium and the zinc ionomer based nanocomposites showed shifts to larger *d* spacings relative to the organoclay, suggesting intercalation of polymer species within the organoclay gallery. On the other hand, the WAXS peaks of nanocomposites prepared from the lithium ionomer shifted to lower *d* spacings, indicating loss of mass from the galleries of the organoclay. On the basis of WAXS analysis, mechanical property data, and melt rheology observations, the lower levels of organoclay exfoliation observed in the nanocomposites prepared from the lithium ionomer are suggested to be a result of the irreversible exchange of quaternary ammonium ions for the very small lithium ions that can enter the montmorillonite lattice structure.

Acknowledgment. The authors sincerely thank Doug Hunter and Southern Clay Products for providing the organoclay and WAXD analyses of the nanocomposites. We also acknowledge Prof. R. A. Register of Princeton University and Prof. K. I. Winey of University of Pennsylvania for providing useful insights into rheological behavior of Surlyn ionomers.

References and Notes

(1) Eisenberg, A.; Kim, J.-S. *Introduction to Ionomers*; Wiley: New York, 1998.
(2) Technical Information, E. I. du Pont de Nemours and Company, http://www.dupont.com/industrial-polymers/plastics/polymers/surlyn.html.
(3) Jerome, R.; Mazurek, M. In *Ionomers*, 1st ed.; Tant, M. R. M., Kenneth, A., Wilkes, G. L., Eds.; Blackie Academic and Professional: London, 1997; pp 3−40.
(4) Manufacturer's information, E. I. du Pont de Nemours and Company, http://www2.dupont.com/Surlyn/en_US/uses_apps/.
(5) Kobayashi, T.; Takahashi, T.; Monma, T.; Kurosaka, K.; Arai, T. WO, 9731973, 1997.
(6) Hasegawa, N.; Kawakado, M.; Usuki, A.; Okada, A. JP, 97-152854, 1998.
(7) Shah, R. K. Ph.D. Thesis, The University of Texas at Austin, 2006.
(8) Ding, R.-d.; Newell, C. US, 6,861,481, 2005.
(9) Barber, G. D.; Calhoun, B. H.; Moore, R. B. *Polymer* **2005**, *46*, 6706−6714.
(10) Barber, G. D.; Bellman, S. P.; Moore, R. B. *Annu. Tech. Conf.—Soc. Plast. Eng.* **2003**, *61st*, 1369−1373.
(11) Chisholm, B. J.; Moore, R. B.; Barber, G.; Khouri, F.; Hempstead, A.; Larsen, M.; Olson, E.; Kelley, J.; Balch, G.; Caraher, J. *Macromolecules* **2002**, *35*, 5508−5516.
(12) Start, P. R.; Mauritz, K. A. *J. Polym. Sci., Part B: Polym. Phys.* **2003**, *41*, 1563−1571.
(13) Kovarova, L.; Kalendova, A.; Malac, J.; Vaculik, J.; Malac, Z.; Simonik, J. *Annu. Tech. Conf.—Soc. Plast. Eng.* **2002**, *60th*, 2291−2295.
(14) Barber, G. D.; Carter, C. M.; Moore, R. B. *Annu. Tech. Conf.—Soc. Plast. Eng.* **2000**, *58th*, 3763−3767.
(15) Shah, R. K.; Hunter, D. L.; Paul, D. R. *Polymer* **2005**, *46*, 2646−2662.
(16) Shah, R. K.; Paul, D. R. *Polymer* **2004**, *45*, 2991−3000.
(17) Fornes, T. D.; Yoon, P. J.; Keskkula, H.; Paul, D. R. *Polymer* **2001**, *42*, 9929−9940.
(18) Fornes, T. D.; Paul, D. R. *Polymer* **2003**, *44*, 4993−5013.
(19) Chavarria, F.; Paul, D. R. *Polymer* **2004**, *45*, 8501−8515.

(20) Lee, H.-s.; Fasulo, P. D.; Rodgers, W. R.; Paul, D. R. *Polymer* **2005**, *46*, 11673−11689.
(21) Winey, K. I. Personal communication.
(22) Register, R. A. Personal communication.
(23) Shah, R. K.; Cui, L.; Williams, K. L.; Bernard, B.; Paul, D. R. *J. Appl. Polym. Sci.*, in press.
(24) Halpin, J. C.; Finlayson, K. M.; Ashton, J. E. *Primer on Composite Materials Analysis*, 2nd rev./ed.; Technomic Pub. Co.: Lancaster, PA, 1992.
(25) Halpin, J. C.; Kardos, J. L. *Polym. Eng. Sci.* **1976**, *16*, 344−352.
(26) Fornes, T. D.; Paul, D. R. *Macromolecules* **2004**, *37*, 7698−7709.
(27) Stretz, H. A.; Paul, D. R.; Cassidy, P. E. *Polymer* **2005**, *46*, 3818−3830.
(28) Fornes, T. D.; Yoon, P. J.; Hunter, D. L.; Keskkula, H.; Paul, D. R. *Polymer* **2002**, *43*, 5915−5933.
(29) Shah, R. K.; Paul, D. R. *Polymer*, in press.
(30) Tanoue, S.; Utracki, L. A.; Garcia-Rejon, A.; Tatibouet, J.; Cole, K. C.; Kamal, M. R. *Polym. Eng. Sci.* **2004**, *44*, 1046−1060.
(31) Xie, W.; Gao, Z.; Pan, W.-P.; Hunter, D.; Singh, A.; Vaia, R. *Chem. Mater.* **2001**, *13*, 2979−2990.
(32) Fornes, T. D.; Yoon, P. J.; Paul, D. R. *Polymer* **2003**, *44*, 7545−7556.
(33) Davis, R.; Gilman, J.; VanderHart, D. *Polym. Degrad. Stab.* **2003**, *79*, 111−121.
(34) Hofmann, U.; Klemen, R. *Z. Anorg. Chem.* **1950**, *262*, 95−99.
(35) Madejova, J.; Bujdak, J.; Gates, W. P.; Komadel, P. *Clay Miner.* **1996**, *31*, 233−241.
(36) Madejova, J.; Bujdak, J.; Petit, S.; Komadel, P. *Clay Miner.* **2000**, *35*, 739−751.
(37) Alvero, R.; Alba, M. D.; Castro, M. A.; Trillo, J. M. *J. Phys. Chem.* **1994**, *98*, 7848−7853.
(38) Theng, B. K. G.; Hayashi, S.; Soma, M.; Seyama, H. *Clays Clay Miner.* **1997**, *45*, 718−723.
(39) Calvet, R.; Prost, R. *Clays Clay Miner., Proc. Conf.* **1971**, *19*, 187−191.
(40) Stackhouse, S.; Coveney, P. V. *J. Phys. Chem. B* **2002**, *106*, 12470−12477.
(41) Williams, J.; Purnell, J. H.; Ballantine, J. A. *Catal. Lett.* **1991**, *9*, 115−119.
(42) Emmerich, K.; Madsen, F. T.; Kahr, G. *Clays Clay Miner.* **1999**, *47*, 591−604.
(43) Emmerich, K.; Plotze, M.; Kahr, G. *Appl. Clay Sci.* **2001**, *19*, 143−154.

MA0600052